Astroparticle Physics 84 (2016) 52–61

Contents lists available at ScienceDirect

Astroparticle Physics

journal homepage: www.elsevier.com/locate/astropartphys

Cascade photons as test of protons in UHECR

V. Berezinsky[a,b], A. Gazizov[a], O. Kalashev[c,*]

[a] INFN, Laboratori Nazionali del Gran Sasso, Assergi (AQ), 67010, Italy
[b] INFN, Gran Sasso Science Institute, viale F.Crispi 7, 67100 L'Aquila, Italy
[c] Institute for Nuclear Research of the Russian Academy of Sciences, Moscow 117312, Russia

ARTICLE INFO

Article history:
Received 3 July 2016
Revised 23 August 2016
Accepted 25 August 2016
Available online 28 August 2016

Keywords:
Ultrahigh energy cosmic rays
Galactic cosmic rays
Cosmic ray theory
Cosmic ray experiment

ABSTRACT

An isotropic component of high energy γ-ray spectrum measured by Fermi LAT constrains the proton component of UHECR. The strongest restriction comes from the highest, $(580-820)$ GeV, energy bin. One more constraint on the proton component is provided by the IceCube upper bound on ultrahigh energy cosmogenic neutrino flux. We study the influence of these restrictions on the source properties, such as evolution and distribution of sources, their energy spectrum and admixture of nuclei. We also study the sensitivity of restrictions to various Fermi LAT galactic foreground models (model B being less restrictive), to the choice of extragalactic background light model and to overall normalization of the energy spectrum. We claim that the γ-ray-cascade constraints are stronger than the neutrino ones, and that however many proton models are viable. The basic parameters of such models are relatively large γ_g and not very large $z_{\max}$. The allowance for He^4 admixture also relaxes the restrictions. However we foresee that future CTA measurements of γ-ray spectrum at $E_\gamma \simeq (600-800)$ GeV, as well as resolving of more individual γ-ray sources, may rule out the proton-dominated cosmic ray models.

1. Introduction

In spite of tremendous technical progress, the long-standing crisis in ultrahigh-energy cosmic rays (UHECR) is not yet settled. In short, the essence of this crisis is the difference in mass compositions at energies above 4 EeV obtained by Pierre Auger observatory (PAO) [1] on the one hand, and HiRes [2] (closed in 2009) and Telescope Array (TA) [3] on the other hand. PAO shows a steadily heavier mass composition with energy increasing starting from protons (or protons and Helium) at $E \simeq 1$ EeV up to heavier nuclei at $E \simeq 30$ EeV. The two other biggest experiments are consistent with a pure proton composition, or maybe with mixed proton + Helium one, at all energies $E \gtrsim 1$ EeV. It should be noted that all three experiments use the same fluorescent light detection technique for measurement of the mass composition.

In this situation indirect methods of the mass composition detection become important, though they cannot dismiss the necessity of direct measurements. In fact, the energy spectrum is strongly involved in the conflict with mass composition.

The pure proton composition leaves remarkable features in the energy spectrum. Propagating through CMB, UHE protons undergo photopion production

$$p + \gamma_{\rm CMB} \to \pi^{\pm,0} + X, \tag{1}$$

and pair-production

$$p + \gamma_{\rm CMB} \to e^+ + e^- + p, \tag{2}$$

which result in a sharp steepening of the spectrum due to Eq. (1) at highest energies, called Greisen–Zatsepin–Kuzmin (GZK) cutoff [4,5], and in a shallow deepening of the spectrum at lower energies owing to (2) called *dip* [6].

Presence of these features in the energy spectrum proves the *proton composition* of UHECR.

All three aforementioned detectors have observed the sharp steepening in the end of the energy spectrum and all three collaborations claim that the observed steepening is consistent with GZK cutoff. But while the steepenings observed by HiRes and TA before 2015 agree well with the theoretically predicted value $E \approx 50$ EeV, namely $E = 56.2 \pm 5.1$ EeV for HiRes and $E = 48 \pm 1.0$ EeV for TA, the cutoff energy in the case of PAO is noticeably lower, $E = 25.7^{+1.1}_{-1.2}$ EeV. For the PAO collaboration, this is an expected result since PAO observes a non-proton mass composition at highest energies.

Before 2015 both HiRes and TA also observed the GZK cutoff in the integral spectrum at $E_{1/2} = 53.7 \pm 8$ EeV, in a good agreement with the theoretical prediction $E_{1/2} \approx 52.5$ EeV [7]. However, in

* Corresponding author. Tel.: +74991352169.
E-mail addresses: venya.berezinsky@lngs.infn.it (V. Berezinsky), askhat.gazizov@lngs.infn.it (A. Gazizov), kalashev@inr.ac.ru (O. Kalashev).

http://dx.doi.org/10.1016/j.astropartphys.2016.08.007
0927-6505/

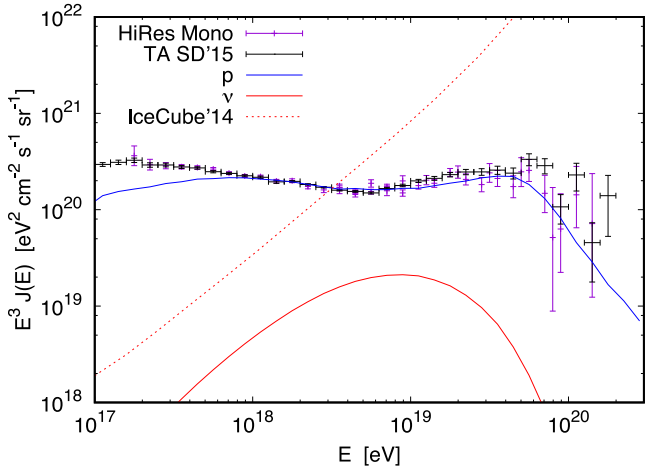

(a) UHECR and secondary ν

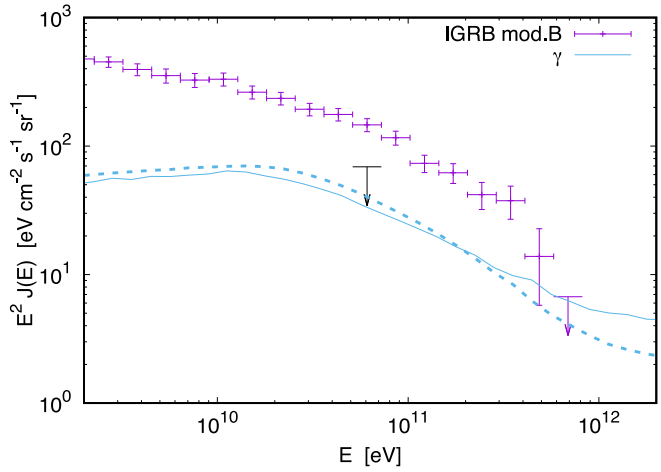

(b) secondary γ

Fig. 1. Energy spectra of protons and neutrinos (left panel) and of cascade photons (right panel) from sources emitting protons with $\gamma_g = 2.6$, $m = 1$ and $z_{\max} = 5$ normalized on TA spectrum [41]. Also, the Fermi IGRB measurements are shown for galactic foreground model B, as well as secondary ν-spectrum along with IceCube neutrino 'differential flux' upper limit [18]. The Fermi LAT constraint of Eq. (13) is shown by the black arrow. EBL models of Ref. [36] (solid lines) and [35] (dashed line) were used in calculations. Only γ-ray spectrum is shown for EBL model [35] since p- and ν-spectra calculated using different EBL models are practically indistinguishable.

new higher statistics data [8] the GZK cutoff is not seen as clearly as before both in differential and in integral spectra.

For the last 20 years, the scientific community was hypnotized by the GZK cutoff, more precisely by its absence. And the glory of this phenomenon left in shadow another feature, the dip, which is also a signature of protons interacting with CMB photons. This feature is quite faint, but it is located at lower, $(1 - 40)$ EeV, energies where statistics is much higher than in the case of GZK cutoff.

Calculated for the ordinary UHECR spectrum, the dip is a model-dependent feature. Its shape depends on many phenomena and parameters, such as the way of propagation (rectilinear or diffusive), index of the generation spectrum γ_g, parameters of cosmological evolution and especially the mass composition. But in terms of *modification factor* $\eta(E)$ [9,10], dip becomes considerably less model-dependent, still remaining different for protons and nuclei.

Defined for protons, the modification factor is a ratio of proton spectrum $J_p(E)$, calculated with all energy losses included, and of so-called unmodified spectrum, $J_{\rm unm}(E)$, which accounts only for adiabatic (due to red-shift) energy loss:

$$\eta(E) = J_p(E)/J_{\rm unm}(E). \tag{3}$$

Modification factor is an excellent tool for *interaction signatures* [11]. According to (3), interactions (1) and (2) enter only the numerator remaining unsuppressed in $\eta(E)$, while most other phenomena entering both the numerator and the denominator are either suppressed or even cancelled in the modification factor.

This property is especially pronounced for the dip modification factor. According to Ref. [9,10], the *theoretical* dip modification factors depend very weakly on generation index γ_g, $E_{\max}$ and on such characteristics as propagation mode, average source separation, local source overdensity or deficit etc. Calculated for different $\gamma_g = 2.0$ and 2.7 (see Fig. 2 of Ref. [9] and Fig. 3 of Ref. [12]), they are practically indistinguishable at all energies.

While cosmological evolution of sources just moderately modifies $\eta(E)$, an admixture of nuclei changes it significantly. Therefore one can define the *dip model* in terms of modification factor as one strongly dominated by protons and with weak cosmological evolution (see Ref.[9] where the evolution is taken as that of AGN in X-ray observations).

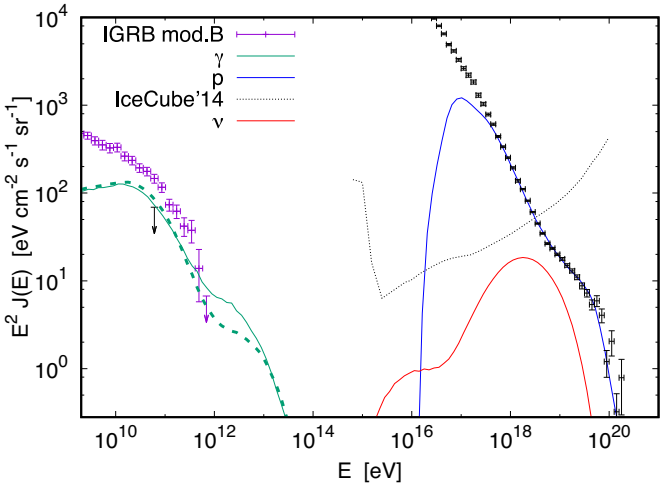

Fig. 2. Energy spectrum of cosmic rays and secondary ν's and γ's from sources emitting protons with $\gamma_g = 2.4$ and evolution corresponding to star formation rate (SFR) [37] normalized on TA spectrum [41]. The Fermi LAT constraint given by Eq. (13) is shown by the black arrow. The EBL models of Refs. [36] (solid lines) and [35] (dashed line) are used in calculations. The γ-ray spectrum is shown only for EBL of model Ref. [35] since $p-$ and ν-spectra calculated using different EBL models are almost indistinguishable.

Above, the theoretical modification factor was discussed. The *observational* modification factor is given by the ratio of the observed flux $J_{\rm obs}(E)$ and unmodified spectrum $J_{\rm unm}(E) \propto E^{-\gamma_g}$. Defined up to normalization constant,

$$\eta_{\rm obs}(E) \propto J_{\rm obs}(E)/E^{-\gamma_g}. \tag{4}$$

Here γ_g is an exponent of the proton generation function $Q_{\rm gen}(E_g) \propto E_g^{-\gamma_g}$ in terms of initial proton energies E_g.

To fit $\eta(E)$ to $\eta_{\rm obs}(E)$ one has just two free parameters, γ_g and the overall normalization factor for $\gtrsim 20$ energy bins of each experiment. The comparison is shown in Fig. 8 of Ref. [9] and Fig. 4 of Ref. [12]. It is clear that both the proton pair-production dip and the beginning of GZK cutoff up to 80 EeV were well confirmed by data of Akeno-AGASA, HiRes, Yakutsk and Telescope Array with data of 2013. And only two free parameters were needed for the

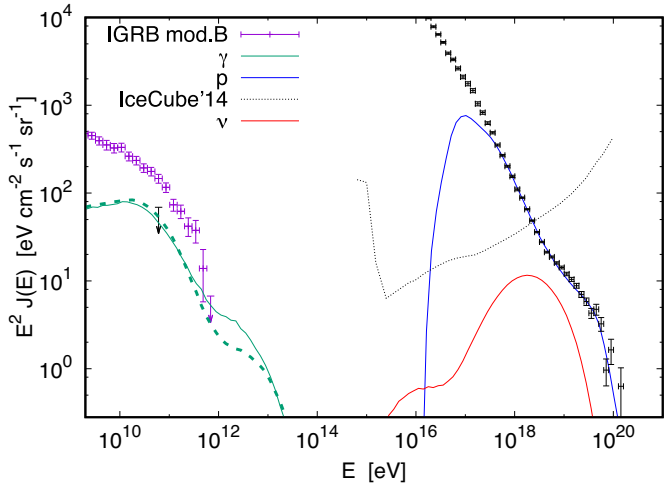

Fig. 3. Same as Fig. 2 but for UHECR spectrum normalized by the TA spectrum with energy scale downshifted by 20%.

description of 20–30 energy bins in each of four experiments. The values of γ_g providing this agreement were fixed as 2.6–2.7.

The ankle observed in all these experiments is well described as dip produced in the pair-production process (2) and not by transition from galactic to extragalactic cosmic rays. So, an excellent confirmation of dip and GZK cutoff in terms of modification factor in all above mentioned experiments evidences for the proton composition of UHECR [12].

Another indirect method to distinguish proton-dominated cosmic ray models from nuclei-dominated ones is given by measurements of *cosmogenic neutrino* flux. Protons are much more efficient in the production of neutrinos than nuclei. Being first proposed in 1969 [13], cosmogenic neutrinos and their production have been studied in many works [14–17]. The observational upper limits on cosmogenic neutrinos have been recently obtained at $E > 10^{16}$ eV in IceCube detector [18,19] and at $E > 10^{17}$ eV in PAO [20]. These upper limits constrain only some extreme models of UHECR with hard injection spectrum, strong evolution and relatively high $z_{\max}$ [21]. Generally, they do not dismiss both proton and nuclei models.

In the present work we study the allowed class of proton UHECR models, which fit the observed UHECR spectrum. We also calculate the diffuse neutrino fluxes for these models. In some cases the produced neutrino flux exceeds the upper limit of IceCube; these models are qualified as excluded. But the majority of models analysed in this paper are allowed by the IceCube upper limit.

And finally, the most severe indirect constraint on proton models is imposed by the observed diffuse γ-radiation. We consider this restriction below, first discussing a specific problem of cosmogenic neutrino and diffuse γ-ray flux. The neutrino flux is directly connected with the diffuse γ-radiation in case it has electromagnetic (EM) cascade nature. The flux of cosmogenic neutrinos is strongly suppressed if the flux of cascade γ-radiation is low. This phenomenon was first noticed in Ref. [22], where a relation between cosmogenic neutrino flux $J_\nu(E)$ and energy density $\omega_{\rm cas}$ of cascade γ-radiation was obtained as

$$E^2 J_\nu(E) < \frac{c}{4\pi}\,\omega_{\rm cas}. \tag{5}$$

In Ref. [23] this formalism was further developed. Using the Fermi EGRB γ-ray flux, it was found that maximum allowed EM cascade energy density $\omega_{\rm cas} = 5.8 \times 10^{-7}$ eV/cm^3. The cosmogenic neutrino flux was found to be below the IceCube upper limit [23], but still detectable in near future [24,25].

The properties of extragalactic diffuse γ-radiation render a powerful tool for distinguishing between proton or nuclei dominances in the UHECR spectrum. This information can be obtained from observation of the energy spectrum of diffuse γ-radiation and its $\omega_{\rm cas}$. A historical development of observations tends to the diminishing of the role of protons as a source of the observed extragalactic diffuse γ-radiation.

The research approach has been initiated by the study of diffuse galactic γ-radiation on SAS-2 satellite. In 1975 it has demonstrated [26] that this radiation is produced by galactic cosmic rays. In the 1990s the EGRET detector on board of Compton Gamma Ray Observatory measured extragalactic diffuse γ-ray emission in energy interval 30 MeV – 100 GeV [27] and detected the extragalactic γ-ray sources, including blazars.

In Refs. [22,28] the EGRET data were used to put upper limits on diffuse fluxes of UHECR and cosmogenic neutrinos. The observed diffuse γ-radiation in these works was interpreted as γ-radiation from EM cascades initiated by protons. The cascade energy spectrum was estimated as $\propto E^{-2}$ [22], in agreement with measured in Ref. [27] gamma-ray spectrum $\propto E^{-\gamma}$ with $\gamma = 2.10 \pm 0.03$. The physical quantity which characterizes UHE neutrinos and CR diffuse flux was given in these calculations by energy density of the cascade radiation $\omega_{\rm cas}$. Using the EGRET data, it as found in Refs. [22,28] that $\omega_{\rm cas} = 5 \times 10^{-6}$ eV/cm^3.

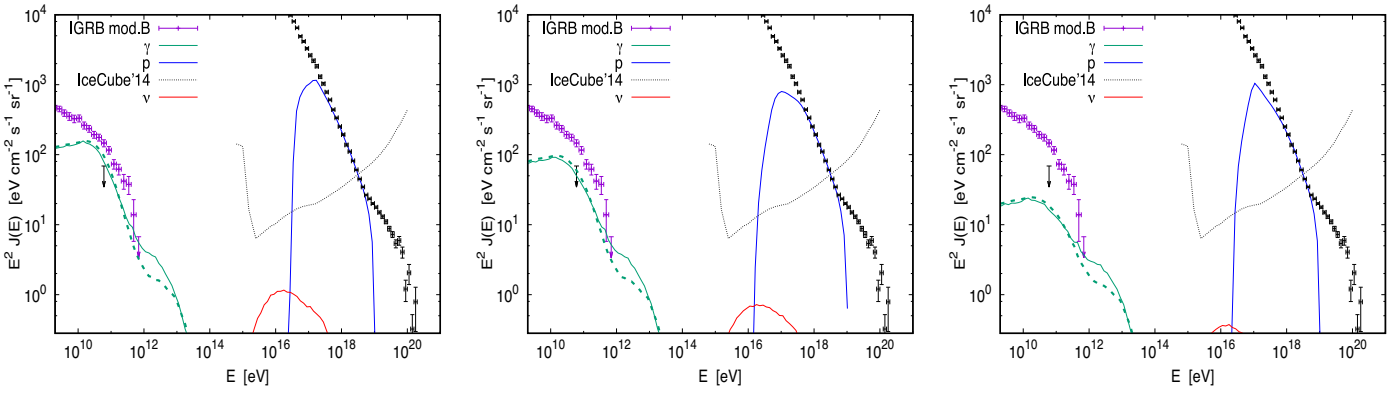

(a) $\gamma_g = 2.1$, $m = 3.9$, $z_{\max} = 2$ (b) $\gamma_g = 2.19$, SFR evolution (c) $\gamma_g = 2.6$, $m = 0$, $z_{\max} = 3$

Fig. 4. Energy spectra of cosmic rays and secondary ν and γ from proton sources with $E_{\max} = 10$ EeV and fitting the TA spectrum [41] in the energy range (1–4)EeV. The Fermi LAT constraint of Eq. (13) is shown by the black arrow. Cascade γ-fluxes calculated using EBL models of Ref. [36] and Ref. [35] are shown by solid and dashed lines, respectively. The cosmic ray and neutrino spectra calculated using either EBL model are almost indistinguishable.

The first 10 months of Fermi-LAT observations [29] have put a stronger limit on the isotropic diffuse gamma-ray background (IGRB) in energy interval 200 MeV – 120 GeV. A more steep index of the power-law spectrum, $\gamma = 2.41 \pm 0.05$, was found. The analysis of Ref [23]. gave lower IGRB and, respectively, lower cascade energy density $\omega_{\rm cas} = 5.8 \times 10^{-7}$ eV/cm^3.

Regular lowering of the $\omega_{\rm cas}$ since the first SAS-2 satellite measurement means the diminishing of γ-ray cascade flux and hence of associated with it UHE proton flux. Analysis [23] of the data including $\omega_{\rm cas}$ in terms of UHECR proton models demonstrates that many proton models survive, though some of them, mostly those with strong cosmological evolution, are excluded.

More stringent limit on proton component of UHECR can be extracted from 50 months observation of Fermi LAT [30]. The limit becomes stronger due to Highest Energy Bin (HEB) at (580 – 820) GeV, where the Fermi-LAT flux is particularly low. This effect is analysed in Refs. [31–33] with rather an extreme conclusion in Ref. [31]. Here we argue that using reasonable galactic foreground in Fermi LAT analysis (model B) and extragalactic background light (EBL) model we keep the proton models alive.

Nevertheless, we admit that isotropic γ-radiation looks like a serious potential problem for models with proton composition. The difference in generation indexes of predicted cascade gamma-ray spectrum $\gamma = 1.9$ and observed by Fermi LAT, $\gamma = 2.4$ shows that proton-induced composition of γ-rays must be much smaller than one observed. There easily could be more unresolved sources in IGRB flux. On the other side, the clearly seen dip and GZK cutoff in modification factor analyses strongly support the proton composition. We expect that future CTA [34] data may radically change the situation.

2. UHECR and cascade radiation

In this section we first construct (Section 2.1) the standard proton models to fit the observed spectra of UHECR and calculate the produced fluxes of the cascade EM radiation. Protons with energies (2 – 20) EeV at present create e^+e^- pairs on CMB photons (2). The produced electrons and positrons initiate EM cascades interacting with EBL and CMB target photons. The spectra of cascading photons are calculated using two methods: by solving kinetic equations and performing MC simulations. The isotropic diffuse γ-ray background measurements by Fermi LAT [30] put the upper limit on the flux of cascade photons. The constraint is especially strong at the highest energy bin, i.e. at (580 – 800) GeV.

The IGRB flux is strongly model-dependent especially at HEB since it is derived by subtraction of the simulated galactic contribution from observational data. We take into account the model dependence by considering all three galactic foreground models originally used in IGRB calculations. The model B leads to highest IGRB estimate and therefore is the least restrictive. We also account for uncertainties in EBL by using two EBL models of Refs.[35] and [36]. As a result, we obtained two tables of main proton source model characteristics, which correspond to two EBL models with different status of the agreement with IGRB flux. The further increase of the number of models which respect the HEB restriction in the two aforementioned tables, may be reached by taking into account the possible systematic errors in measured energies of UHECR. Shifting the whole energy spectrum downwards results in decreasing of e^+e^- production rate, so that more models become allowed.

In Section 2.2, following Ref. [31], we address a question whether the proton component observed at (1 – 4) EeV in all experiments (HiRes, TA, and Auger) contradicts to Fermi LAT IGRB flux. For this purpose we construct auxiliary models with cutoffs at high and low energies to imitate spectrum in the discussed (1 – 4) EeV energy range. We find that in many cases the observed proton flux at (1 – 4) EeV is allowed by the Fermi LAT IGRB. A contradiction with Ref. [31] is mainly explained by using of model B for galactic contribution in the Fermi LAT experiment.

In Section 2.3 we analyze the proton component with nuclei admixture in the form of Helium. The basic idea behind this proposal is that experimentally He^4 is difficult to tell from protons. Helium is less efficient in the production of e^+e^- pairs and thus the cascade flux is suppressed. In fact, the situation is more complicated and different for hard and soft generation spectra. For small generation indexes, e.g. $\gamma_g = 2.1$ the secondary proton component from Helium photo-disintegration is comparable with the primary proton flux and thus the γ-ray component is suppressed but a little. For large generation indexes, e.g. $\gamma_g = 2.6$, the secondary protons from Helium decay are strongly suppressed and thus Helium-produced flux of photons is small. However, extra component is required in this case to fit the UHECR observations above 4 EeV.

In Section 2.4 we calculate the red-shift distribution of points of cascade γ-ray production and redshift distribution of parent protons in the models of $p\gamma$-production of the primaries for cascade photons.

2.1. Standard proton models

We consider simple phenomenological models of homogeneously distributed sources emitting ultrahigh energy protons with power-law generation spectra

$$Q_p(E,z) \propto n(z)\left(\frac{E}{E_0}\right)^{-\gamma_g}, \quad E \in [E_{\rm min}, E_{\rm max}], \tag{6}$$

where E_0 is an arbitrary normalization energy. Below unless we state explicitly, we cut the injection spectrum below $E_{\rm min} = 0.1$ EeV and above $E_{\rm max} = 10^{2.5}$ EeV without loss of generality. Indeed the main contribution to the EM cascade comes from protons with energies in the interval from 1 EeV to a few EeV unless the injection spectrum is too flat ($\gamma_g \le 2$) which is forbidden anyway as it will be demonstrated below. Also note, that models with $E_{\rm max} > 10^{2.5}$ EeV don't substantially improve UHECR fit but may overproduce secondary ν-flux. We also introduce the evolution of source density with redshift z given by the term $n(z)$ assuming however that the source spectrum shape does not depend on z. For the evolution term we use a general form

$$n(z) = n(0)(1+z)^{3+m} \quad \text{for } 0 \le z \le z_{\rm max}, \tag{7}$$

where the case of $m = 0$ corresponds to the constant comoving source density. We also consider a specific case of source density proportional to the star formation rate (SFR) [37]:

$$n_{\rm SFR}(z) \propto (1+z)^3 \begin{cases} (1+z)^{3.4}, & z \le 1 \\ (1+z)^{-0.3}, & 1 < z \le 4 \\ (1+z)^{-3.5}, & z > 4. \end{cases} \tag{8}$$

With these assumptions and with γ_g varying in a wide range 2 – 2.7, we include in consideration a large class of models used in literature.

During propagation to an observer, protons lose their energy through pion (1) and e^+e^--pair production (2) on CMB and EBL. Both processes give rise to EM cascades since secondary electrons and photons are produced with energies above the threshold for e^+e^--pair production. High energy photons are produced by inverse Compton $e^\pm$ scattering off CMB photons

$$e^\pm + \gamma_{\rm CMB} \to e^\pm + \gamma, \tag{9}$$

and new high energy $e^\pm$ pairs arise in

$$\gamma + \gamma_{\rm CMB,EBL} \to e^+ + e^- \tag{10}$$

collisions of γ-rays with CMB and EBL.

This chain of reactions proceeds until photons become sterile forming the diffuse γ-ray background, and the latter can be compared with the measurements of Fermi LAT [30]. We simulate propagation of protons and development of secondary EM cascades using the code of Refs. [8,25] that allows solving transport equations in 1D. The solutions are double-checked by an independent Monte Carlo code previously used in Ref. [33].

Although energy density of EBL is $\sim$ 15 times lower than that of CMB, the EBL photons play a crucial role in attenuation of EM cascades below the pair production threshold on CMB, i.e. at $E_\gamma \lesssim$ 100 TeV. The EBL energy spectrum has a characteristic two-bump shape with a near-infrared bump at $\sim$ 1 eV produced by direct starlight emission and a far-infrared bump at the energy around 0.01 eV produced by starlight scattering off dust. Direct measurements provide just an upper bound on the EBL intensity because of a much stronger foreground of zodiacal light from the Solar system; the latter is to be subtracted from observations. The lower bounds on the EBL intensity may be estimated using source counts in deep observations by infrared and optical telescopes.

The present upper and lower bounds on EBL at different wavelengths are summarized in Fig. 7 of Ref. [38]. In the literature, there are additional constraints of EBL based on observations of distant blazars. These bounds were derived using the attenuation of photons without an account for the possible contribution of secondary γ-ray signal from protons; it means that these constraints may be relaxed [39]. The limits based on GRBs [40] observations remain unaffected, however, they are only applicable to the highest energy part of EBL spectrum.

In this work we use one of the latest EBL model by Inoue et al. [36] which is close to the minimal estimate. In parallel we use the popular model of Kneiske et al. [35] that provides a larger EBL density. It will be shown that the choice of EBL model has a noticeable effect on the cascade flux.

Among the cosmic ray models we look for those providing reasonable fits to the telescope array [41] and HiRes [42] spectra. The energy spectra of both detectors are in a good agreement, and both observe the mass composition compatible with pure protons.

It is important to note that we do not require the perfect fitting of the cosmic ray data, especially in terms of best χ^2. The reasons are as follows:

- at present, the systematic errors in all UHECR experiments are much larger than the statistical ones,
- demanding the best fit can be too limiting for the *exclusion* of some hypotheses,
- we use just simple phenomenological source models, e.g. assuming their homogeneous distribution,
- we consider pure proton models, while an admixture of nuclei is quite possible; this is especially true for Helium nuclei, which are difficult to distinguish experimentally from protons.

With the above assumptions, we are able to construct reasonable fits to data with sufficiently high $E_{\max}$ and power-law indexes in the range $2 \le \gamma_g \le 2.7$, and to choose appropriate evolution parameter m in Eq. (7) in the range $0 \le m \le 7$. To fit UHECR data at $E \sim (1-10)$ EeV , the harder injection spectra require the stronger evolution (for illustration see e.g. Fig. 4a of Ref. [25]). The choice of $z_{\max}$ has a weak effect on UHECR spectrum, provided that $z_{\max} \gtrsim 1$, but it does have the effect on fluxes of secondary γ-rays and neutrinos produced in this model.

We should also note that hard injection spectra in combination with strong evolution bring to a proton flux exceeding the KASCADE-Grande measurements [43]. We do not deny such models since the average extragalactic injection spectrum may have a broken power-law form. It may be also suppressed even stronger below 1 EeV, for example, because of sources distribution in maximal energies [44]. Otherwise, to avoid proton overproduction at $E \lesssim 1$ EeV, one should assume lower maximum red-shifts, $z_{\max} \lesssim 0.7$.

Table 1
Maximal ratios η_γ, $\tilde{\eta}_\gamma$ for galactic γ-ray foreground models A, B or C for several representative proton source models fitting TA spectrum. The ratios higher than 1 are in conflict with Fermi LAT data. Also shown the expectation value of the neutrino events $\bar{N}_\nu$ with energy $E_\nu > 10$ PeV assuming IceCube 7 year exposure from Fig. 1 of Ref. [19]. Models with $\bar{N}_\nu > 2.3$ have Poisson probability less than 10%. All spectra are calculated using the EBL model of Ref. [36].

γ_g	m	$z_{\max}$	η_γ ($\tilde{\eta}_\gamma$) [A]	η_γ ($\tilde{\eta}_\gamma$) [B]	η_γ ($\tilde{\eta}_\gamma$) [C]	$\bar{N}_\nu$
2.6	1	5	1.40 (0.59)	0.94 (0.50)	1.11 (0.57)	0.78
2.6	1	1	1.38 (0.46)	0.93 (0.39)	1.10 (0.44)	0.31
2.5	2	5	1.60 (0.87)	1.07 (0.74)	1.26 (0.84)	2.24
2.5	2	1	1.57 (0.60)	1.05 (0.51)	1.24 (0.58)	0.48
2.4	SFR	5	1.88 (1.20)	1.26 (1.03)	1.49 (1.16)	2.28
2.3	5	1	2.23 (1.38)	1.49 (1.18)	1.76 (1.33)	1.72
2.2	6	1	2.52 (1.86)	1.69 (1.59)	2.00 (1.79)	2.88
2.2	5	0.7	2.15 (0.83)	1.44 (0.71)	1.70 (0.80)	0.99
2.2	6	0.7	2.31 (0.99)	1.55 (0.85)	1.83 (0.95)	1.19

The Fermi LAT collaboration has presented the measurements of isotropic gamma-ray background, IGRB, and of the total extragalactic gamma-ray background (EGB), the latter being composed of IGRB and the flux from resolved extragalactic sources [30]. The EGB flux is in turn calculated by subtraction of galactic foreground from observational data.

We normalize proton models by fitting the TA spectrum and compare the calculated integral fluxes of the cascade γ-radiation, Φ_i^{cas}, with the IGRB integral flux $\Phi_i^{\rm IGRB}$ in each energy bin of the Fermi LAT diffuse background data. Namely, for each bin i we calculate ratios

$$\eta_i = \Phi_i^{\rm cas}/\Phi_i^{\rm IGRB}.$$

These ratios have maximum in some bin i' and we introduce the value η_γ as

$$\eta_\gamma = \max(\Phi_i^{\rm cas}/\Phi_i^{\rm IGRB}). \tag{11}$$

A strong criterion for the model consistency with data is given by

$$\eta_\gamma \le 1. \tag{12}$$

Most often (but not always !) the criterion of consistency takes place in the highest energy bin, where $\Phi_i^{\rm IGRB}$ has minimum.

An analysis of the recent Fermi LAT data [45] shows that a considerable fraction of EGB events with energies above 50 GeV may be attributed to unresolved γ-ray sources, mostly to blazars. According to this analysis, the contribution of blazars to EGB flux reaches 86^{+16}_{-14}%. This implies even stronger bound on the true isotropic flux

$$\tilde{\eta}_\gamma \equiv \frac{\int_{50GeV}^{\infty} \Phi_\gamma^{\rm cas}(E)dE}{0.28\int_{50GeV}^{\infty} \Phi_{\rm EGB}(E)dE} \le 1. \tag{13}$$

The denominator of Eq. (13) stands for true isotropic integral flux calculated under an assumption of minimal contribution from all resolved and unresolved blazars. At 1σ approximation its fraction is just $0.86 - 0.14 = 0.72$ of the total EGB flux. In this case, the fraction of isotropic component in EGB is $1 - 0.72 = 0.28$, as it is included in the denominator of Eq. (13).

In Tables 1 and 2 the maximal fractions η_γ and $\tilde{\eta}_\gamma$ are shown for several representative models. The models with $\eta_\gamma > 1$ or $\tilde{\eta}_\gamma > 1$ are in contradiction with the Fermi LAT data. In this case the $\min(1/\eta_\gamma, 1/\tilde{\eta}_\gamma)$ could be roughly interpreted as a maximal allowed fraction of protons in the source spectrum. To be conservative, for the Fermi LAT IGRB and EGB fluxes we use upper limits on the flux allowed by statistical and instrumental errors. We also take into account the uncertainties in galactic foreground by considering all three models, A, B and C, used for derivation of IGRB in Ref. [30].

Table 2
The same values as in Table 1 but calculated using the EBL model of Ref. [35].

γ_g	m	z_{max}	η_γ ($\tilde{\eta}_\gamma$) [A]	η_γ ($\tilde{\eta}_\gamma$) [B]	η_γ ($\tilde{\eta}_\gamma$) [C]	$\bar{N}_\nu$
2.6	1	5	0.92 (0.66)	0.61 (0.57)	0.73 (0.64)	0.78
2.6	1	1	0.90 (0.48)	0.60 (0.41)	0.71 (0.47)	0.31
2.5	2	5	1.02 (1.03)	0.68 (0.89)	0.81 (1.00)	2.24
2.5	2	1	0.99 (0.63)	0.66 (0.54)	0.79 (0.61)	0.48
2.4	SFR	5	1.16 (1.34)	0.78 (1.15)	0.92 (1.30)	2.28
2.3	5	1	1.29 (1.47)	0.87 (1.26)	1.02 (1.42)	1.72
2.2	6	1	1.42 (2.00)	0.95 (1.71)	1.17 (1.93)	2.88
2.2	5	0.7	1.30 (0.87)	0.87 (0.75)	1.03 (0.84)	0.99
2.2	6	0.7	1.35 (1.04)	0.91 (0.89)	1.07 (1.01)	1.19

In addition, we calculate all-flavor flux of cosmogenic neutrinos, arising from decays of pions and neutrons produced in $p\gamma$-collisions, and the expectation value for the number of neutrino events $\bar{N}_\nu$ with energy $E_\nu > 10$ PeV, where no events have been observed so far. For this we use the recently published IceCube exposure [19] for 7 years of observation and assume neutrino flavour ratio after propagation (1:1:1), which is roughly true for cosmogenic neutrinos. The values of $\bar{N}_\nu$ are shown in the last column of Table 1. The models with $\bar{N}_\nu > 2.3$ have Poisson likelihood less than 10%.

Table 1 clearly shows that IGRB measurements provide a significant constraint for the UHECR models with protons as primaries. In the case of minimal EBL [36] only models with soft enough injection spectra, $\gamma_g \gtrsim 2.6$, and weak evolution $m \leq 1$ survive the IGRB constraint. This tension may be avoided in the case of galactic foreground model B, which predicts a lower γ-ray flux.

With EBL of Ref. [35] (see Table 2) more models survive the γ-ray constraint, though SFR evolution model is still excluded.

It is interesting to note that the results presented in columns 5 and 6 of Table 2 show the agreement of UHECR models with Fermi LAT flux in the case of galactic subtractions B or C and $\gamma_g \geq 2.5$. Moreover, the condition (12) is fulfilled even for harder injection spectra while condition (13) in this case may be satisfied only by constraining maximal source redshift $z_{max} \lesssim 0.7$.

In Fig. 1 we show the spectra of cosmic rays and secondaries (high energy γ's and ν's) from their interactions with CMB and EBL in the model with $\gamma_g = 2.6$ and $m = 1$. The upper limit at 50 GeV shown in Fig. 1b is the constraint of Eq. (13) due to unresolved sources [45].

We see that in the case of minimal EBL flux of cascade photons is very close to the Fermi LAT upper bound in the highest energy IGRB bin assuming galactic foreground model B. Note that for A and C models, which predict higher contributions of galactic foreground and therefore lower IGRB flux, the resulting cascade photon flux produced by UHE protons exceeds the IGRB flux in the last energy bin.

In Fig. 2 we show the model with $\gamma_g = 2.4$ and SFR evolution which almost saturates the allowed flux of the cascade photons for the EBL model of Ref. [36]. Summarizing results presented in Tables 1 and 2 first of all one notes that the strongest constraints are provided by HEB in the Fermi LAT spectra. The constraints depend strongly on the galactic subtraction model A, B, and C used in the Fermi LAT analysis, and on model of the EBL (we use two models Refs. [36] and [35]). For exclusion of each UHECR model one must choose EBL providing the lowest calculated flux and the highest Fermi LAT flux. To be conservative about unresolved source Fermi LAT flux we consider both Eq. (12) and Eq. (13).

From Tables 1 and 2 we see that some pure proton composition models with $\gamma_g \leq 2.5$ fitting entire CR spectrum are excluded by Fermi LAT fluxes.

One way to relax this tension is to shift the experimental data energy scale downwards by an amount allowed by systematic errors. In all existing UHECR experiments, the systematic errors in energy determination are quite large. In the case of TA data, these errors are $\sim$ 20% [41]. We estimate the effect of systematic errors by fitting TA SD spectrum with energy scale shifted by 20% towards lower energies. It is naturally expected that $E^{-\gamma}$ spectrum shifted downwards produces fewer cascade photons because of diminishing the number of protons at the threshold of e^+e^- pair-production. The results of our calculations are presented in Tables 3 and 4. One can see that more models indeed become acceptable in this case, in particular those with SFR evolution for both galactic foregrounds B and C. The comparison of this model with Fermi LAT and IceCube data is shown in Fig. 3.

Table 3
Maximal ratios η_γ, $\tilde{\eta}_\gamma$ (assuming galactic γ-foreground models A, B or C) for several representative proton source models fitting TA spectrum with energy scale downshifted by 20%. The ratios higher than 1 are in conflict with secondary Fermi LAT IGRB flux measurements. Also shown the expectation value of the neutrino events $\bar{N}_\nu$ with energy $E_\nu > 10$ PeV assuming IceCube 7 year exposure from Fig. 1 of Ref. [19]. Models with $\bar{N}_\nu > 2.3$ have Poisson probability less than 10%. The spectra are calculated using EBL model of Ref. [36].

γ_g	m	z_{max}	η_γ ($\tilde{\eta}_\gamma$) [A]	η_γ ($\tilde{\eta}_\gamma$) [B]	η_γ ($\tilde{\eta}_\gamma$) [C]	$\bar{N}_\nu$
2.6	0	5	0.80 (0.26)	0.53 (0.23)	0.63 (0.26)	0.26
2.6	0	1	0.79 (0.23)	0.53 (0.20)	0.63 (0.22)	0.15
2.5	2	5	1.00 (0.54)	0.67 (0.46)	0.79 (0.52)	1.40
2.5	2	1	0.98 (0.37)	0.66 (0.32)	0.78 (0.36)	0.30
2.4	SFR	5	1.18 (0.76)	0.79 (0.65)	0.94 (0.73)	1.43
2.4	3	5	1.16 (0.87)	0.77 (0.75)	0.92 (0.84)	5.00
2.3	4	1	1.29 (0.67)	0.86 (0.57)	1.02 (0.64)	0.81
2.2	5	1	1.47 (0.90)	0.98 (0.77)	1.16 (0.87)	1.34
2.2	5	0.7	1.38 (0.53)	0.92 (0.46)	1.09 (0.51)	0.64
2.2	6	0.7	1.46 (0.62)	0.98 (0.53)	1.15 (0.60)	0.75

Table 4
Same as Table 3 but calculated using EBL model of Ref. [35].

γ_g	m	z_{max}	η_γ ($\tilde{\eta}_\gamma$) [A]	η_γ ($\tilde{\eta}_\gamma$) [B]	η_γ ($\tilde{\eta}_\gamma$) [C]	$\bar{N}_\nu$
2.6	0	5	0.53 (0.29)	0.36 (0.25)	0.42 (0.28)	0.26
2.6	0	1	0.53 (0.24)	0.35 (0.20)	0.42 (0.23)	0.15
2.5	2	5	0.64 (0.65)	0.43 (0.56)	0.51 (0.63)	1.40
2.5	2	1	0.62 (0.39)	0.42 (0.34)	0.49 (0.38)	0.30
2.4	SFR	5	0.73 (0.84)	0.49 (0.72)	0.58 (0.82)	1.43
2.4	3	5	1.27 (1.13)	0.87 (0.97)	1.12 (1.09)	5.00
2.3	4	1	0.77 (0.71)	0.52 (0.61)	0.61 (0.68)	0.81
2.2	5	1	0.86 (0.96)	0.57 (0.82)	0.68 (0.93)	1.34
2.2	5	0.7	0.83 (0.56)	0.56 (0.48)	0.66 (0.54)	0.64
2.2	6	0.7	0.85 (0.66)	0.57 (0.56)	0.67 (0.63)	0.75

2.2. (1 – 4) *EeV band*

All biggest detectors agree that mass composition in the energy range (1 – 4) EeV is light. The consistency of this result can be tested independently by calculation of the secondary cascade radiation. In the recent work Ref. [31] authors found a contradiction between the assumption of pure proton composition in the discussed energy range and the Fermi LAT IGRB data.

In fact, γ-ray production in the discussed energy range is related to the generation rate of protons at early times, i.e. at large redshifts z, and thus it is model dependent. In this subsection we demonstrate that there are models in which the γ-ray radiation from the existing (1 – 4) EeV proton band, and from production by protons at larger z, does not exceed the Fermi LAT limit. In our calculations we construct the models fitting total cosmic ray flux just in the (1 – 4) EeV energy band, and predicting the flux which is less than the observed one outside this energy range. For this we introduce artificial cutoffs in the generation rate at energies above and below (1 – 4) EeV (see Fig. 4).

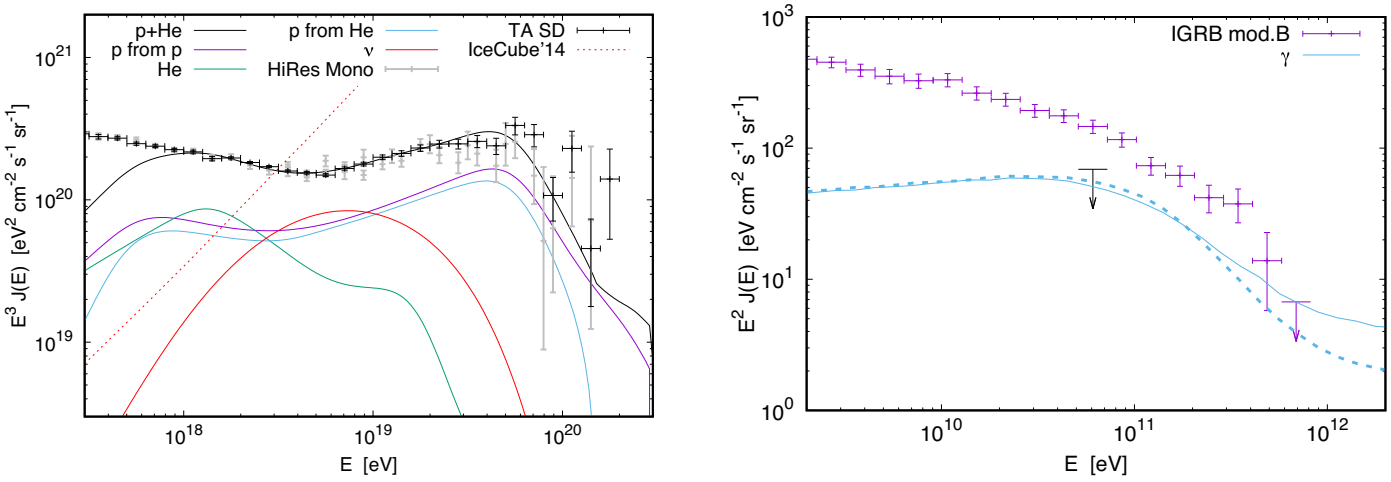

(a) Cosmic Rays (b) Secondary γ's

Fig. 5. Energy spectrum of cosmic rays, secondary neutrinos (left panel) and cascade photons (right panel) from sources emitting mixture of protons (48%) and He (52%) with $\gamma_g = 2.1$, $m = 5$ and $z_{\max} = 1$ normalized on TA spectrum [41]. The constraint of Eq. (13) is shown by the black arrow (right panel). γ-ray spectra are shown for EBL models of Ref. [36] (solid line) and [35] (dashed line). Cosmic ray and ν-spectra are shown only for EBL of Ref. [35].

In calculations below we use only two additional assumptions: the Fermi LAT galactic component is that of model *B*, and the EBL is one of two models, Ref. [36] or Ref. [35]. We made the calculations for the two extreme values of generation indexes $\gamma_g = 2.6$ and $\gamma_g = 2.1$ as well as for the representative case of SFR evolution. The calculated γ-flux together with Fermi LAT upper limits are shown in Fig. 4. One may see that in this case fewer models are constrained by Fermi LAT. In particular, SFR evolving sources are not excluded even without shifting experimental energy scale. This is an expected result since by cutting injection at $E_{\max} = 10$ EeV we have also decreased the contribution to EM component. Interestingly, the model with hard injection spectrum $\gamma_g = 2.1$ and evolution stronger than of SFR, shown in Fig. 4a, is prohibited only by constraint Eq. (13) and formally satisfies the Fermi LAT IGRB bound.

Thus we conclude that pure proton contents of the observed $(1-4)$ EeV energy band produces the γ-radiation which, at least in some models, is below the Fermi LAT upper limit.

2.3. Admixture of nuclei

Nuclei are less efficient in production of photons and one may think that if some nuclei are erroneously taken in the experiment as protons, the calculated γ-ray production is overestimated as a prediction. The realistic picture is more complicated.

The most natural case is given by Helium nuclei, which is difficult to distinguish experimentally from protons.

First, following two papers by Aloisio et al. [46,47], we describe shortly the He^4 photo-disintegration life-time in terms of the Lorentz-factors. The steepening of spectrum at small Lorentz factor occurs at $\Gamma_c = 4 \times 10^8$ due to the transition from adiabatic energy losses to photo-disintegration on EBL. The most noticeable spectrum feature, the Gerasimova–Rozental cutoff [48], occurs at Lorentz factor $\Gamma_c = 4 \times 10^9$ where the transition from photo-disintegration on EBL and CMB takes place.

The photo-disintegration of Helium is followed by very fast decays of the produced secondary nuclei He^3, *T*, *D* and neutron. Hence an assumption that photo-disintegration of He^4 is instantaneously followed by the production of four protons gives a realistic description at both spectrum steepenings, $\Gamma_c = 4 \times 10^8$ and $\Gamma_c = 4 \times 10^8$.

The e^+e^- pair-production energy loss plays just a minor role in the formation of spectrum shape, but this particular process is responsible for photon production. As was demonstrated in Ref. [46,47], the rate of Lorentz-factor loss $\Gamma^{-1}d\Gamma/dt$ satisfies the following relation for nuclei *A* and proton *p* components

$$\left(\frac{1}{\Gamma}\frac{d\Gamma}{dt}(\Gamma)\right)_A = \frac{Z^2}{A}\left(\frac{1}{\Gamma}\frac{d\Gamma}{dt}(\Gamma)\right)_p. \tag{14}$$

Thus the rate of energy loss for He^4 with $Z^2/A = 1$ is equal to that of a proton if $\Gamma_A = \Gamma_p$, i.e. for nucleus energy *A* times higher than that of the proton. It means that at equal energies $E_A = E_p$ the rate of energy loss $(1/E)(dE/dt)$ for the nucleus is less than that for the proton and thus nuclei produce less cascade photons than protons.

Therefore, in the case of Helium one expects two competing effects in comparison with protons: i) diminishing of the pair-production energy loss at the same energy and ii) production of four protons with 4 times lower energy (still active in photon emission) in the prompt processes of Helium photo-disintegration. The latter process must work more efficiently for the hard generation spectra.

Below we shall discuss two cases of the mixed composition of protons and Helium.

The energy spectrum of pure Helium is characterized by the cutoff at energy $E \sim 1 \times 10^{18}$ eV due to photo-disintegration on EBL, which looks like a maximum in the traditional presentation of spectrum in the form $E^3J(E)$. To describe the observed spectrum up to $\sim$ 100 EeV one needs another component which in $p + He$ mixing models is given by protons.

In Fig. 5 we present the $p + He$ model with almost extreme mixing which fits the observed spectrum with the ratio of the production rates $Q_p/Q_{He} = 0.9$. This model is characterized by generation index $\gamma_g = 2.1$, evolution parameters $m = 5$, $z_{\max} = 1$ and maximum of acceleration $E_{\max} = Z \times 300$ EeV, where *Z* is the charge. The observed dip in the energy spectrum is produced by He bump at $E \simeq 1.4$ EeV superimposed on the proton dip. One can notice that flux of the secondary protons from photo-disintegration of He^4 is practically equal to the flux of primary protons. The sum of these components provides the main contribution to the cascade photons, while the direct contribution from He^4 is negligible. The

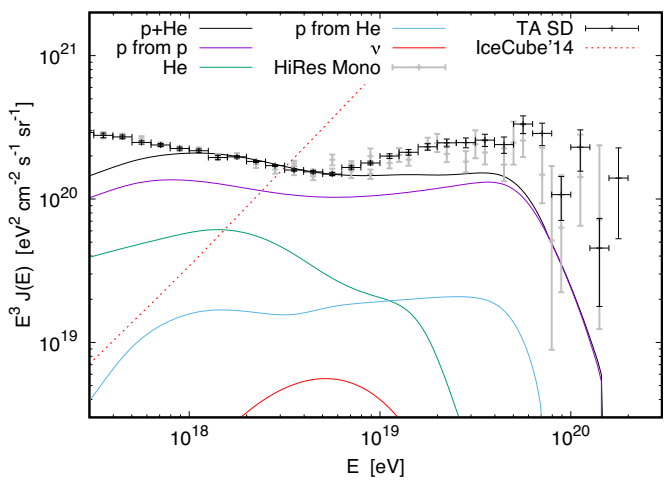

(a) Cosmic Rays

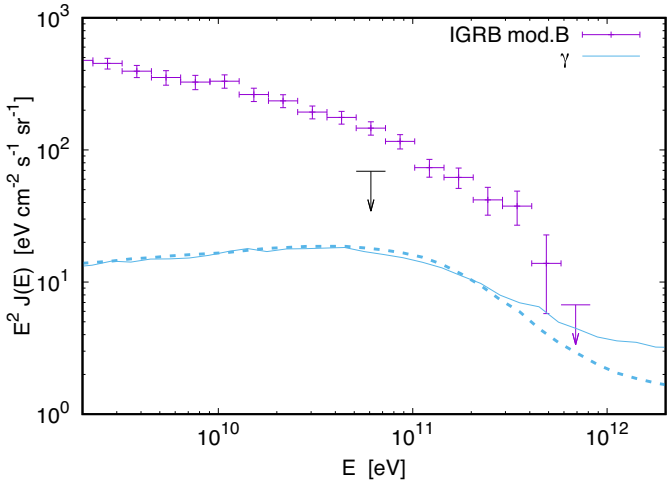

(b) Secondary γ

Fig. 6. Energy spectrum of cosmic rays, secondary neutrinos (left panel) and cascade photons (right panel) from sources emitting protons with 30% admixture of He with $\gamma_g = 2.6$, $E_{\max} = Z \times 150$ EeV, $m = 1$ and $z_{\max} = 1$ normalized on TA spectrum [41]. The Fermi constraint given by Eq. (13) is shown by the black arrow (right panel). γ-ray spectra are shown for EBL models of Ref. [36] (solid line) and [35] (dashed line). Cosmic ray and ν spectra are only shown for EBL of Ref. [35].

flux of cascade photons produced in the Fermi HEB in this model is 36% less than one predicted by the pure proton source model with the same injection spectrum.

In Fig. 6 we present calculations for soft proton and He production spectra with $\gamma_g = 2.6$. It is clear that in this case the production of secondary protons is suppressed; the direct photon production by Helium is suppressed too for the general reason discussed above. This model fails to fit the observational data above 10 EeV, but it allows to suppress the flux of cascade photons by 26% compared to pure proton source case. To get a reasonable fit to the data one should diminish the He content to very a low level, where suppression of cascade photon flux is approximately equal to the fraction of He in the generation flux.

2.4. Sources and magnetic fields

In case the proton component is the dominant one in UHECR, the observation of cascade radiation, and in particular the Fermi LAT observations at present, give information about sources of UHECR. The photons observed in HEB of Fermi LAT cannot arrive from large redshifts and thus the sources of UHE protons being parents of photons from HEB, cannot lie at too large distances. However, the distribution of protons, the parents of HEB photons, should be wider than that of photons because of their larger interaction length.

In Fig. 7 the red solid line shows the spectrum of the cascade photons produced in the typical model of pure proton sources explaining the observations of TA. In this figure we also show the contribution of proton sources, located at different redshift ranges, to the total γ-ray flux. These fluxes are compared with HEB of Fermi LAT data [30]. One may see that cascade flux in the Fermi LAT HEB $(580 - 820)$ GeV is mostly produced by sources with redshifts $z < 0.4$, while the cosmologically distant sources, those with $z > 0.8$, have a weak effect on the last bin.

Fig. 8 presents the redshift distribution of protons and cascade photons contributing to HEB of the Fermi LAT experiment in the discussed model. Interestingly, one can see that while the UHE proton sources may be distant, the EM cascades are initiated relatively nearby at $z \lesssim 0.1$. This is because photons of HEB are absorbed at larger distances on EBL radiation, but the parent protons can cross this distance and produce photons close to the observer

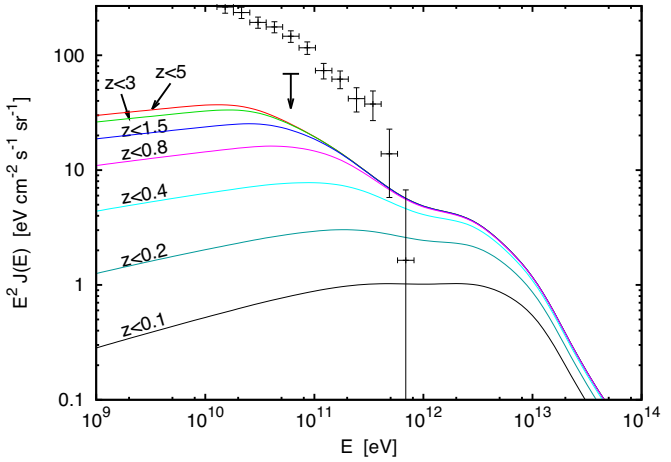

Fig. 7. Cascade photon spectrum from UHE protons with source injection function $E^{-2.7}$, $m = 0$ and $z_{\max} = 5$ normalized on TA energy spectrum. Contributions from different redshift ranges of proton production are shown. Also, the Fermi LAT IGRB measurement (model B) and constraint of Eq. (13) are shown with black error bars and arrow respectively.

[39]. HEB photons are produced nearby: the maximum of the distribution is located at $z_\gamma^{\max} \simeq 0.01$ with the mean redshift of the distribution $< z_\gamma >= 0.09$. The distribution of parent protons production redshift is wider and is shifted towards higher redshift: $z_p^{\max} = 0.1$ and $< z_p >= 0.21$.

The results which we have obtained above might in principle depend on the assumption about the strength of intergalactic magnetic field (IGMF) which is currently poorly known. Indeed, we assume that secondary γ-ray flux from UHECR protons is isotropic in the entire energy range where IGRB is measured and most importantly in the last energy bin $E_\gamma \lesssim 1$ TeV. However, as it was shown in Ref. [39], the TeV secondary γ-rays may point back to their sources provided that IGMF strength is less than 10^{-14} G. Such events would not contribute to IGRB but to total EGB flux and therefore one may argue that IGRB bound is irrelevant in this case. However, the more detailed consideration reveals that just 6 resolved sources (5 BL Lacs and one of unknown type) with galac-

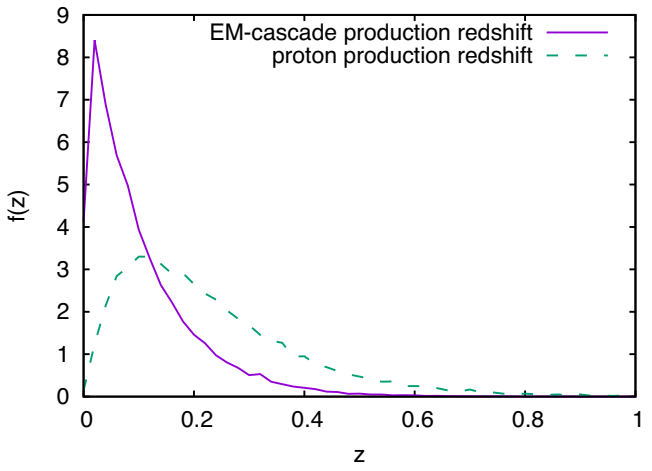

Fig. 8. The distribution of protons (dashed line) and secondary EM cascade (solid line) production redshifts contributing to the last Fermi LAT energy bin for the UHECR model used in Fig 7.

tic latitude $|b| > 20^\circ$ and redshift $z \leq 0.212$ from 2FHL catalog of Fermi LAT [49] constitute 100% of the resolved source flux in the last energy bin of EGB. At the same time sources of UHECR are known to be much more numerous. Indeed, the lack of statistically significant clustering of cosmic rays arrival directions at small scales leads to a lower limit on the local density of UHECR sources $n > 10^{-4}$ Mpc^{-3} [50,51] or roughly 10^5 sources with $z < 0.21$. This means that at least in the last energy bin, which is the most important for us, UHECR sources contribute mostly to IGRB, and EGB bound is irrelevant for them regardless of the level of IGMF.

3. Discussion

Modern UHECR experiments in which mass composition of UHECR is measured using atmospheric shower properties such as depth of shower maximum, result in contradictory conclusions. For this reason the indirect methods facilitating discrimination of various UHECR composition models obtain the considerable importance. In this work we use the method based on calculation of diffuse fluxes of secondary γ-rays and neutrinos generated by UHECR during their propagation. We consider first the models with pure proton composition which are consistent with TA and HiRes data and then the mixed composition of protons and Helium with different ratios. These models include also the dip model which explains the observed feature, the dip at $(1-40)$ EeV by e^+e^- pair production. We demonstrate that many proton models are severely constrained by the Fermi LAT IGRB observations, but there are many models that successfully survive. The first selection of the proton-dominated models follows from the condition of describing the TA or HiRes energy spectra; among these models we choose those with generation indexes γ_g, $z_{\max}$ and cosmological evolution $(1+z)^m$ up to maximum redshift $z_{\max}$ which do not overproduce the Fermi LAT γ-ray radiation.

In the case of unshifted TA spectrum only models with $\gamma_g \geq 2.5$ and relatively weak evolution $m \leq 2$ survive.

The class of surviving models becomes larger when the model B of galactic γ-ray radiation is used in the Fermi LAT analysis and also when the model [35] is used for EBL. The class of allowed models becomes further wider with TA energy scale shifted by 20% towards lower energies (allowed by systematic errors) the constraint weakens to $\gamma_g \geq 2.2$ and $m \leq 5$ assuming $z_{\max} = 1$ or to $\gamma_g \geq 2.4$ and $m \leq 3$ assuming $z_{\max} = 5$ which also includes models with SFR evolution. Limiting maximal source redshift to a value $z_{\max} \leq 0.7$ allows to include models with $m \leq 6$ and $\gamma_g \geq 2.1$.

Models with strong evolution, which require hard injection spectra and sufficiently large $z_{\max}$, are constrained also by the neutrino flux measurements of the IceCube detector [19]. However in most cases modern IGRB constraints on secondary diffuse γ-ray flux are more restrictive than the IceCube limit.

All modern experiments show the light nuclei composition in the energy range $(1-4)$ EeV. Inspired by this observations we consider ad hoc the proton source models fitting UHECR spectrum only in the above-indicated energy range. The cascade γ-ray flux obtained for such models is also very close to the IGRB constraints. In particular, the models with $\gamma_g \leq 2.1$ and $m > 3.5$ normalized on TA overproduce cascade photons. However, as we demonstrated in Section 2.3, an admixture of Helium allows to further decrease the cascade γ-ray flux.

When this paper was in preparation two interesting articles on the similar subject appeared in arXiv: Refs. [31,32]. Both of them are more pessimistic about proton scenarios which in our opinion is due to disregarding the uncertainties in the Fermi LAT data (using the maximal galactic foreground model A) and in UHECR data (systematic errors), uncertainties in EBL models and neglecting of the highly possible admixture of He^4 nuclei to "pure proton models", particularly in the $(1-4)$ EeV energy band.

We would like to comment on interesting analysis in Ref. [31] concerning the energy range $(1-4)$ EeV, where the authors assume the pure proton mass composition and found the excess of γ-radiation over IGRB. The authors argue that local source overdensity or even galactic sources are required to avoid contradiction to Fermi data. We think that this problem and its solution are premature at present. As was demonstrated above, the contradiction may be avoided by using lower galactic foreground (model B) in Fermi LAT, or by higher EBL, or by shifting experimental energy scale within the allowed systematic errors.

The case of pure proton composition in the energy range $(1-4)$ EeV, like in Ref. [31], can be illustrated by Fig. 4 for three values of $\gamma_g = 2.1,\ 2.19$ and 2.6, and for different cosmological evolution. In all three cases when the EBL high-flux model of Ref. [35] is used (the dashed lines for calculated γ-ray spectra in Fig. 4a, b and c) the calculated fluxes are well below the IGRB Fermi LAT upper limit.

Another option not listed above is given by admixture of Helium in the source spectrum, which can be easily mistaken in observations for protons. This case is illustrated by Fig. 6 where we show the UHECR and secondary γ-ray spectra in the source model with 30% Helium admixture. As it was noticed in Ref. [10], the presence of a considerable admixture of nuclei distorts the shape of the dip. In the figure we fit only the energy range $(1-4)$ EeV as in Ref. [31]. The cascade γ-radiation spectrum in this case is compatible with the Fermi IGRB bound.

We finally conclude that measurements of the diffuse gamma-radiation at $E \sim 1$ TeV is a very powerful method to constrain the fraction of protons in UHECR spectrum. Nowadays, with available statistics and poor knowledge of the galactic diffuse foreground and EBL, it is impossible to exclude the pure or almost pure proton composition at $(1-40)$ EeV. However some tension between predictions and observations of gamma-radiation already exists, especially in the highest energy bin; it can be considered as a warning signal and hence a motivation for consideration of alternative solutions.

The discussed problem will be one of the important tasks for the future CTA [34].

Acknowledgments

Work of OK was supported by the Russian Science Foundation, grant 14-12-01340. OK is grateful to GSSI and LNGS for hospitality.

References

[1] A. Aab, et al., Depth of maximum of air-shower profiles at the Pierre Auger observatory. II. Composition implications, Phys. Rev. D90 (12) (2014) 122006, doi:10.1103/PhysRevD.90.122006.

[2] Y. Fedorova, HiRes stereo cosmic rays composition measurements, in: Proceedings, 30th International Cosmic Ray Conference (ICRC 2007), vol. 4, 2007, pp. 463–466. http://indico.nucleares.unam.mx/contributionDisplay.py?contribId=1236&confId=4.

[3] R.U. Abbasi, et al., Study of ultra-High energy cosmic ray composition using Telescope Array's middle drum detector and surface array in hybrid mode, Astropart. Phys. 64 (2015) 49–62, doi:10.1016/j.astropartphys.2014.11.004.

[4] K. Greisen, End to the cosmic ray spectrum? Phys. Rev. Lett. 16 (1966) 748–750, doi:10.1103/PhysRevLett.16.748.

[5] G.T. Zatsepin, V.A. Kuzmin, Upper limit of the spectrum of cosmic rays, JETP Lett. 4 (1966) 78–80. [Pisma Zh. Eksp. Teor. Fiz.4,114(1966)]

[6] G.R. Blumenthal, Energy loss of high-energy cosmic rays in pair-producing collisions with ambient photons, Phys. Rev. D1 (1970) 1596–1602, doi:10.1103/PhysRevD.1.1596.

[7] V.S. Berezinsky, S.I. Grigor'eva, A bump in the ultrahigh-energy cosmic ray spectrum, Astron. Astrophys. 199 (1988) 1–12.

[8] O.E. Kalashev, E. Kido, Simulations of ultra high energy cosmic rays propagation, J. Exp. Theor. Phys. 120 (5) (2015) 790–797, doi:10.1134/S1063776115040056.

[9] V. Berezinsky, A.Z. Gazizov, S.I. Grigorieva, On astrophysical solution to ultrahigh-energy cosmic rays, Phys. Rev. D74 (2006) 043005, doi:10.1103/PhysRevD.74.043005.

[10] R. Aloisio, V. Berezinsky, P. Blasi, A. Gazizov, S. Grigorieva, B. Hnatyk, A dip in the UHECR spectrum and the transition from galactic to extragalactic cosmic rays, Astropart. Phys. 27 (2007) 76–91, doi:10.1016/j.astropartphys.2006.09.004.

[11] V. Berezinsky, A.Z. Gazizov, S.I. Grigorieva, Dip in UHECR spectrum as signature of proton interaction with CMB, Phys. Lett. B612 (2005) 147–153, doi:10.1016/j.physletb.2005.02.058.

[12] R. Aloisio, V. Berezinsky, A. Gazizov, Transition from galactic to extragalactic cosmic rays, Astropart. Phys. 39–40 (2012) 129–143, doi:10.1016/j.astropartphys.2012.09.007.

[13] V.S. Berezinsky, G.T. Zatsepin, Cosmic rays at ultrahigh-energies (neutrino?), Phys. Lett. B28 (1969) 423–424, doi:10.1016/0370-2693(69)90341-4.

[14] R. Engel, D. Seckel, T. Stanev, Neutrinos from propagation of ultrahigh-energy protons, Phys. Rev. D64 (2001) 093010, doi:10.1103/PhysRevD.64.093010.

[15] O.E. Kalashev, V.A. Kuzmin, D.V. Semikoz, G. Sigl, Ultrahigh-energy neutrino fluxes and their constraints, Phys. Rev. D66 (2002) 063004, doi:10.1103/PhysRevD.66.063004.

[16] G. Decerprit, D. Allard, Constraints on the origin of ultrahigh energy cosmic rays from cosmogenic neutrinos and photons, Astron. Astrophys. 535 (2011) A66, doi:10.1051/0004-6361/201117673.

[17] P. Desiati, IceCube observatory: neutrinos and the origin of cosmic rays (2012). arXiv:1210.7703

[18] A. Ishihara, Neutrino astronomy (Rapporteur talk), in: Proceedings, 34th International Cosmic Ray Conference (ICRC 2015), 2015. http://inspirehep.net/record/1404133/files/arXiv:1511.03820.pdf

[19] M.G. Aartsen, et al., Constraints on ultra-high-energy cosmic ray sources from a search for neutrinos above 10 PeV with IceCube(2016). arXiv:1607.05886

[20] J. Abraham, et al., Upper limit on the diffuse flux of UHE tau neutrinos from the Pierre Auger observatory, Phys. Rev. Lett. 100 (2008) 211101. arXiv:0712.1909, doi: 10.1103/PhysRevLett.100.211101.

[21] J. Heinze, D. Boncioli, M. Bustamante, W. Winter, Cosmogenic neutrinos challenge the cosmic ray proton dip model (2015). arXiv:1512.05988

[22] V.S. Berezinsky, A.Yu. Smirnov, Cosmic neutrinos of ultra-high energies and detection possibility, Astrophys. Space Sci. 32 (1975) 461–482, doi:10.1007/BF00643157.

[23] V. Berezinsky, A. Gazizov, M. Kachelriess, S. Ostapchenko, Restricting UHECRs and cosmogenic neutrinos with Fermi-LAT, Phys. Lett. B695 (2011) 13–18. arXiv:1003.1496, doi: 10.1016/j.physletb.2010.11.019.

[24] M. Ahlers, L.A. Anchordoqui, M.C. Gonzalez-Garcia, F. Halzen, S. Sarkar, GZK neutrinos after the Fermi-LAT diffuse photon flux measurement, Astropart. Phys. 34 (2010) 106–115. arXiv:1005.2620, doi: 10.1016/j.astropartphys.2010.06.003.

[25] G.B. Gelmini, O. Kalashev, D.V. Semikoz, Gamma-ray constraints on maximum cosmogenic neutrino fluxes and UHECR source evolution models, JCAP 1201 (2012) 044. arXiv:1107.1672, doi: 10.1088/1475-7516/2012/01/044.

[26] C.E. Fichtel, R.C. Hartman, D.A. Kniffen, D.J. Thompson, G.F. Bignami, H. Oegelman, M.E. Ozel, T. Tumer, High-energy galactic gamma radiation observed by the SAS-2 satellite (1975).

[27] P. Sreekumar, et al., EGRET observations of the extragalactic gamma-ray emission, Astrophys. J. 494 (1998) 523–534. arXiv:astro-ph/9709257, doi: 10.1086/305222

[28] V.S. Berezinsky, Neutrino astronomy and massive longlived particles from big bang, Nucl. Phys. B380 (1992) 478–506, doi:10.1016/0550-3213(92)90255-A.

[29] A.A. Abdo, et al., The spectrum of the isotropic diffuse gamma-ray emission derived from first-Year Fermi large area telescope data, Phys. Rev. Lett. 104 (2010) 101101. arXiv:1002.3603, doi: 10.1103/PhysRevLett.104.101101

[30] M. Ackermann, et al., The spectrum of isotropic diffuse gamma-ray emission between 100 MeV and 820 GeV, Astrophys. J. 799 (2015) 86. arXiv:1410.3696, doi: 10.1088/0004-637X/799/1/86

[31] R.-Y. Liu, A.M. Taylor, X.-Y. Wang, F.A. Aharonian, Evidence for a local "Fog" of sub-ankle UHECR(2016). arXiv:1603.03223.

[32] E. Gavish, D. Eichler, On ultra high energy cosmic rays and their resultant gamma rays, Astrophys. J. 822 (1) (2016) 56. arXiv:1603.04074, doi: 10.3847/0004-637X/822/1/56.

[33] V. Berezinsky, O. Kalashev, High energy electromagnetic cascades in extragalactic space: physics and features (2016). arXiv:1603.03989.

[34] M. Actis, et al., Design concepts for the Cherenkov Telescope Array CTA: an advanced facility for ground-based high-energy gamma-ray astronomy, Exp. Astron. 32 (2011) 193–316. arXiv:1008.3703, doi: 10.1007/s10686-011-9247-0.

[35] T.M. Kneiske, T. Bretz, K. Mannheim, D.H. Hartmann, Implications of cosmological gamma-ray absorption. 2. Modification of gamma-ray spectra, Astron. Astrophys. 413 (2004) 807–815. arXiv:astro-ph/0309141, doi: 10.1051/0004-6361:20031542.

[36] Y. Inoue, S. Inoue, M.A.R. Kobayashi, R. Makiya, Y. Niino, T. Totani, Extragalactic background light from hierarchical galaxy formation: gamma-ray attenuation up to the epoch of cosmic reionization and the first stars, Astrophys. J. 768 (2013) 197. arXiv:1212.1683, doi: 10.1088/0004-637X/768/2/197.

[37] H. Yuksel, M.D. Kistler, J.F. Beacom, A.M. Hopkins, Revealing the high-Redshift star formation rate with gamma-ray bursts, Astrophys. J. 683 (2008) L5–L8. arXiv:0804.4008, doi: 10.1086/591449.

[38] E. Dwek, F. Krennrich, The extragalactic background light and the gamma-ray opacity of the universe, Astropart. Phys. 43 (2013) 112–133. arXiv:1209.4661, doi: 10.1016/j.astropartphys.2012.09.003.

[39] W. Essey, O.E. Kalashev, A. Kusenko, J.F. Beacom, Secondary photons and neutrinos from cosmic rays produced by distant blazars, Phys. Rev. Lett. 104 (2010) 141102. arXiv:0912.3976, doi: 10.1103/PhysRevLett.104.141102.

[40] A.A. Abdo, et al., Fermi large area telescope constraints on the gamma-ray opacity of the universe, Astrophys. J. 723 (2010) 1082–1096. arXiv:1005.0996, doi: 10.1088/0004-637X/723/2/1082.

[41] R.U. Abbasi, et al., The energy spectrum of cosmic rays above $10^{17.2}$ ev measured by the fluorescence detectors of the Telescope Array experiment in seven years, Astropart. Phys. 80 (2016) 131–140. arXiv:1511.07510, doi: 10.1016/j.astropartphys.2016.04.002.

[42] R.U. Abbasi, et al., First observation of the Greisen-Zatsepin-Kuzmin suppression, Phys. Rev. Lett. 100 (2008) 101101. arXiv:astro-ph/0703099, doi: 10.1103/PhysRevLett.100.101101.

[43] J.C. Arteaga-VelÈâÃízquez, et al., The KASCADE-Grande observatory and the composition of very high-energy cosmic rays, J. Phys. Conf. Ser. 651 (1) (2015) 012001, doi:10.1088/1742-6596/651/1/012001.

[44] M. Kachelriess, D.V. Semikoz, Reconciling the ultra-high energy cosmic ray spectrum with Fermi shock acceleration, Phys. Lett. B634 (2006) 143–147. arXiv:astro-ph/0510188, doi: 10.1016/j.physletb.2006.01.009.

[45] M. Di Mauro, The origin of the Fermi-LAT γ-ray background, 14th Marcel Grossmann Meeting on Recent Developments in Theoretical and Experimental General Relativity, Astrophysics, and Relativistic Field Theories (MG14) Rome, Italy, July 12–18, 2015, 2016. http://inspirehep.net/record/1415711/files/arXiv:1601.04323.pdf.

[46] R. Aloisio, V. Berezinsky, S. Grigorieva, Analytic calculations of the spectra of ultra-high energy cosmic ray nuclei. I. The case of CMB radiation, Astropart. Phys. 41 (2013) 73–93. arXiv:0802.4452, doi: 10.1016/j.astropartphys.2012.07.010.

[47] R. Aloisio, V. Berezinsky, S. Grigorieva, Analytic calculations of the spectra of ultra high energy cosmic ray nuclei. II. The general case of background radiation, Astropart. Phys. 41 (2013) 94–107. arXiv:1006.2484, doi: 10.1016/j.astropartphys.2012.06.003.

[48] N.G. Gerasimova, I.L. Rozental, Interaction of nuclei and photons of high energies with a thermal radiations in the universe, JETP 41 (1961) 488.

[49] M. Ackermann, et al., 2FHL: The second catalog of hard Fermi-LAT sources, Astrophys. J. Suppl. 222 (1) (2016) 5. arXiv:1508.04449, doi: 10.3847/0067-0049/222/1/5.

[50] S.L. Dubovsky, P.G. Tinyakov, I.I. Tkachev, Statistics of clustering of ultrahigh energy cosmic rays and the number of their sources, Phys. Rev. Lett. 85 (2000) 1154–1157. arXiv:astroph/0001317, doi: 10.1103/PhysRevLett.85.1154.

[51] P. Abreu, et al., The Pierre Auger observatory III: other astrophysical observations, in: Proceedings, 32nd International Cosmic Ray Conference (ICRC 2011), 2011. http://inspirehep.net/record/919729/files/arXiv:1107.4805.pdf